



Control of hysteretic instability in rotating machinery by elastic suspension systems subject to dry and viscous friction

Francesco Sorge*, Marco Cammalleri

Department of Mechanics, University of Palermo, Viale delle Scienze, 90128 Palermo, Italy

ARTICLE INFO

Article history:

Received 10 July 2009

Received in revised form

27 October 2009

Accepted 4 December 2009

Handling Editor: H. Ouyang

Available online 13 January 2010

ABSTRACT

Most of the undesired whirling motions of rotating machines can be efficiently reduced by supporting journal boxes elastically and controlling their movement by viscous dampers or by dry friction surfaces normal to the shaft axis, which rub against the frame. In the case of dry dampers, resonance ranges of the floating support configuration can be easily cut off by planning a motionless adhesive state of the friction surfaces. On the contrary, the dry friction contact must change automatically into sliding conditions when the fixed support resonances are to be feared. Moreover, the whirl amplitude can be restrained throughout the speed range by a proper choice of the suspension-to-shaft stiffness ratio and of the support-to-rotor mass ratio.

This theoretical research deals firstly with the natural precession speeds and looks for Campbell plots in dependence on the shaft angular speed, for several rotor-suspension systems. Then, the steady response to unbalance is investigated, in terms of rotor and support orbits and of conical path of the rotor axis. In this search, the ranges of adhesive or sliding contact are identified in particular for system with dry friction damping. At last, the destabilizing influence of the shaft hysteresis in the supercritical regime is focalized and the counterbalancing effect of the other dissipative sources is verified. In the nonlinear case of dry friction dampers, the control of linear stability is fulfilled by a perturbation procedure, checking the magnitude of Floquet characteristic multipliers on the complex plane. Moreover, the nonlinear stability far from steady motion is tested by the direct numerical solution of the full motion equations. The comparison configuration of suspension systems with viscous dampers and no dry friction is examined through an analytical first approximation approach and closed-form results for stability thresholds are derived in particular for the symmetric case.

© 2009 Elsevier Ltd. All rights reserved.

1. Introduction

It is known that very noxious whirling motions may arise in a rotor-shaft-support system on approaching critical flexural speeds, and a great deal of previous studies have been focusing on this technical problem and on the strategies to face it. For example, annular motion-limiting stops or squeeze-film dampers may restrain the whirling motions, or else compliant supports may improve the frequency response, though increasing the number of critical speeds. Flexible-damped supports have been widely proposed (see for example [1–4]), taking advantage of a behaviour more or less similar

* Corresponding author. Tel.: +39 091 6657157; fax: +39 091 6657163.

E-mail addresses: sorge@dima.unipa.it (F. Sorge), cammalleri@dima.unipa.it (M. Cammalleri).

Nomenclature**A** flexibility matrix $c_{1,3,4}$ (N s/m), c_2 (N s/m), c_h (N s/m) translative, rotative, and hysteretic coefficients of damping $d_{1,3,4}$, d_2 , d_h translative, rotative, and hysteretic damping factors**D** damping matrix e (m) rotor eccentricity EI (Nm²) shaft flexural stiffness**F_h** (N) hysteretic force on rotor h (N/m) hysteresis constant**H** hysteresis matrix j_a, \tilde{j}_a (kg m²) diametral and axial moment of inertia of rotor $J_d = j_d / (ml^2)$, $J_a = \tilde{j}_a / (ml^2)$ dimensionless diametral and axial moment of inertia of rotor k (N/m) reference shaft stiffness k_3, k_4 (N/m) suspension stiffness**K** stiffness matrix $K_3 = k_3/k$, $K_4 = k_4/k$ dimensionless suspension stiffness l (m) shaft length $L_3 = -z_3/l$, $L_4 = z_4/l$ dimensionless distances of rotor from supports m (kg) rotor mass m_3, m_4 (kg) support mass**M** mass matrix $M_3 = m_3/m$, $M_4 = m_4/m$ dimensionless support mass R_1, R_2, R_3, R_4 dimensionless steady amplitudes of rotor path (1), tilt (2), and of support paths (3,4) $\tilde{\mathbf{U}}, \tilde{\mathbf{V}}$ speed perturbation vectors \mathbf{v}_{rel} (m/s) relative velocity vector $\mathbf{W}(\theta)$ complex displacement-rotation vector \mathbf{W}_0 complex amplitude vector x, y, z, x_0, y_0, z_0 (m) coordinates in non-rotating references**X, Y** displacement-rotation vectors**Z** complex impedance matrix $\Gamma = mg/(ek)$ dimensionless gravity field δ_j perturbation of d_j , scaled by d_h $\theta = \omega t$ angular time variable λ perturbation of Ω_n , scaled by d_h $\xi, \eta, \zeta, \xi_0, \eta_0, \zeta_0$ (m) coordinates in rotating references σ (=1 or 0) sliding or adhesion indicator φ, ψ small rotation angles around x and y due to shaft bending Φ, Φ_{adh} (N) sliding and adhesion friction forces $\Phi = \phi/(ek)$, $\Phi_{adh} = \phi_{adh}/(ek)$ dimensionless sliding and adhesion friction forces $\hat{\Phi}_{adh}$ complex dimensionless adhesion force ω (s⁻¹) angular speed $\omega_c = k/m$ (s⁻¹) reference critical speed $\Omega = \omega/\omega_c$ dimensionless angular speed $\Omega_n = \omega_n/\omega_c$ dimensionless whirling speed of natural mode

Subscripts and superscripts

1 rotor centre displacement

2 rotor tilt

3 back support displacement

4 front support displacement

(...) ^(c) cofactor(...)', (...)' first, second derivative with respect to θ

~ perturbation variable

to viscous-dynamic vibration absorbers. Nevertheless, such additional sources of dissipation remain active and absorb power also at the nominal operating point, even far from the critical speeds.

Previous analyses of the authors have developed the idea of suspending the journal boxes on elastic supports and providing them with suitable dry friction surfaces orthogonal to the shaft axis, which rub against the frame and have the task of damping the critical whirling motion [5,6]. The wear compensation of the sliding surfaces can be made in practice automatic by installing suitable spring devices to load the friction pads (e.g. Belleville washers, which may keep the closure force nearly constant when properly designed). Systems of this type have been patented in the past [7,8], but an in-depth analysis has not yet been carried out so far.

This suspension configuration operates most efficiently if the adhesive state is planned for an extended portion of the speed range, including the usual working condition of the rotating machine, while the sliding conditions are allowed to start spontaneously and quench the whirling motions when approaching the critical speeds of the fixed-support system. The dry friction dampers behave thus similarly to automatic clutches, which either lock or release the connection between the journal boxes and the frame depending on the rotational speed, and do not produce a relevant increase of power dissipation or heat production as a whole, because the operating point lies in the adhesive range, where the friction devices are stuck and the supports motionless. These results can be obtained by a careful choice of the dry friction level, of the suspension-to-shaft stiffness ratio, and of the support-to-rotor mass ratio.

On the other hand, a rather significant drawback of rotating machinery is the trend for unstable whirling conditions in the range above the first critical speed, because of the shaft structural friction associated with material hysteresis [9,10]. More broadly, Ref. [11] classifies circulatory systems with non-conservative positional forces (e.g. of hysteretic origin) and non-dissipative systems with gyroscopic terms, showing how their marginal stability may be destroyed when all effects are present together (see [11] also for a survey on the literature). These undesired phenomena may be counteracted by other dissipative sources and may be dealt with by introducing an equivalent coefficient of viscous damping, dependent on the whirling frequency, and imposing that the hysteretic force is given by the product of this coefficient and the rotor centre velocity relative to a reference frame rotating with the shaft end section. This permits calculation of the influence of hysteresis on the gravitational equilibrium configuration and on the overall system response in the speed range.

The stability conditions in the presence of hysteresis and of other dissipative sources may be analyzed by applying the small perturbation approach to the steady motion. If the system behaviour is nonlinear due to the dry friction forces, the slightly perturbed motion equations come out to contain time-varying periodic coefficients, whence the Floquet approach has to be used, checking the magnitude of the Floquet characteristic multipliers. Furthermore, the nonlinear stability far from the steady solutions can be ascertained by the direct numerical solution of the motion equations, e.g. by some Runge–Kutta routine. The result is that the dry friction on the supports produces a strong stabilizing effect and, in case of linear instability, yields non-periodic trajectories that are very close to the steady orbits. In the linear case of viscous dampers, the perturbation approach produces simpler formulas that can be handled for the calculation of the stability threshold.

2. Outline of the mathematical model

2.1. Equations of motion

The mathematical model is similar to that in [6] and will be briefly described here. The dry friction forces on the suspension induce a strong nonlinearity because of their continuous self-aligning in opposition to the variable direction of the instantaneous sliding velocity. Nevertheless, steady circular solutions may be obtained in closed form for axisymmetric stiffness of the shaft and the supports. The whirling paths become elliptical for anisotropic suspension elasticity [12], which complicates their calculation remarkably.

Fig. 1 shows a scheme of the rotor-suspension system, including viscous and dry friction dampers. The mass centre C is eccentric with respect to the intersection O_1 of the shaft line with the rotor cross-section. The translating frame $Cxyz$ remains parallel to the fixed reference $Ox_0y_0z_0$, while the tilting frame $C\xi\eta\zeta$ does not take part in the main rotating motion with angular speed ω , but performs only small elastic rotations φ and ψ around the axes x and y , due to the shaft bending. The gravitational field g is counter-directed with respect to the y -axis.

The translational and rotational motions of the rotor are supposed to be affected by some external environmental dissipation and then the viscous equivalent coefficients c_1 and c_2 are introduced, assuming that the correspondent resistant force and moment are proportional to the translating and tilting velocities of the rotor, respectively. Likewise, the coefficients c_3 and c_4 are used to describe some possible viscous damping on the back and front supports.

Introducing a reference stiffness k of the shaft (e.g. $k=48EI/l^3$ for self-aligning bearings) and a reference natural speed $\omega_c = \sqrt{k/m}$, the dimensionless ratios $\Omega = \omega/\omega_c$, $M_3 = m_3/m$, $M_4 = m_4/m$, $K_3 = k_3/k$, $K_4 = k_4/k$, and the damping factors $d_{1,3,4} = 0.5c_{1,3,4}\omega_c/k$ and $d_2 = 0.5c_2\omega_c/(kl^2)$ are defined. The gravity influence is expressed by means of the dimensionless gravity parameter $\Gamma = mg/(ek)$.

The shaft hysteresis produces an internal resistant force, which acts on the rotor in opposition to the relative velocity v_{rel} of point O_1 with respect to a reference frame $O_3\xi_0\eta_0\zeta_0$ rotating with the shaft angular speed ω around the ζ_0 -axis,

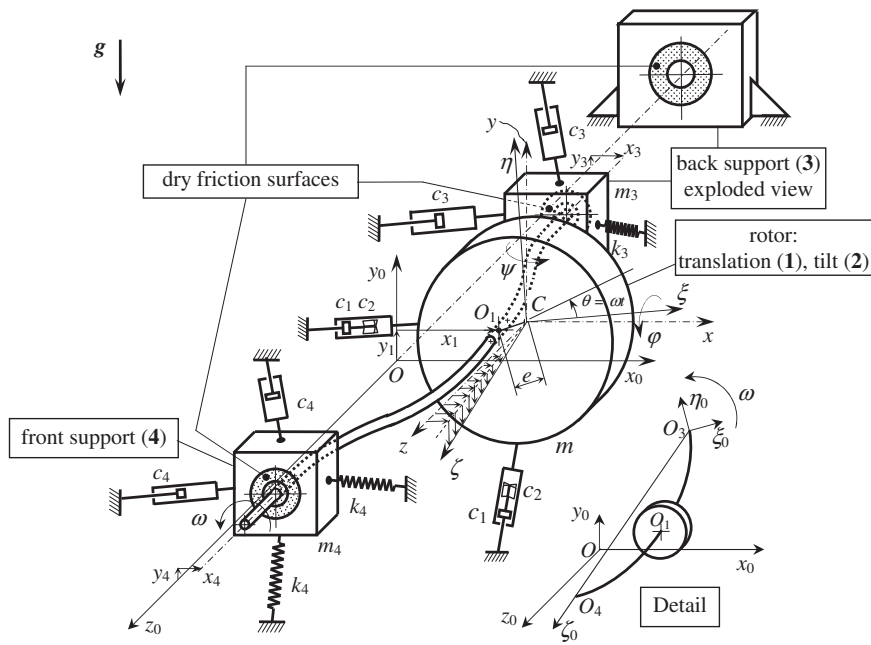


Fig. 1. Scheme of rotating machine with exploded view of back support and frame. The front frame is not represented in the figure. Detail: reference system rotating with end sections.

where ζ_0 passes through the centres of the shaft end sections (see Detail in Fig. 1). In the case of a shaft on two supports, indicating with $L_3 = -z_3/l$ and $L_4 = z_4/l$ the dimensionless distances of the rotor from the shaft ends, the components of \mathbf{v}_{rel} in the fixed reference $Ox_0y_0z_0$ are $v_{rel,x} = \dot{x}_1 - \dot{x}_3L_4 - \dot{x}_4L_3 + \omega(y_1 - y_3L_4 - y_4L_3)$ and $v_{rel,y} = \dot{y}_1 - \dot{y}_3L_4 - \dot{y}_4L_3 - \omega(x_1 - x_3L_4 - x_4L_3)$. The hysteresis force on the rotor is expressed by the product of this velocity and a hysteretic coefficient c_h : $\mathbf{F}_h = -c_h\mathbf{v}_{rel}$, while the forces on the supports are $\mathbf{F}_{3h} = -L_4\mathbf{F}_h$, $\mathbf{F}_{4h} = -L_3\mathbf{F}_h$.

Considering a weighty, horizontal, perfectly balanced rotor in steady motion, the equilibrium deflection plane is motionless but counter-rotates with the angular speed $-\omega$ with respect to the rotating frame $O_3\xi_0\eta_0\zeta_0$ of Fig. 1. Thus, assuming that the hysteretic work is proportional to the cycle area, i.e. that the integral

$$c_h \oint (v_{rel,x}^2 + v_{rel,y}^2) dt = c_h \omega \oint [(y_1 - L_4y_3 - L_3y_4)^2 + (x_1 - L_4x_3 - L_3x_4)^2] d\theta$$

is proportional to the square of the path radius of point O_1 in the rotating frame $O_3\xi_0\eta_0\zeta_0$, one concludes that the product $h = c_h\omega$ may be considered as independent of ω . Therefore, h can be defined as the hysteresis constant of the shaft material and a constant hysteretic factor $d_h = 0.5h/k$ may be also introduced. When some unbalance is added to the rotor, either static or dynamic, a further shaft deflection is superimposed, on a plane that rotates together with the shaft at the same angular speed ω , so that this new deflection is uninfuential on the hysteretic work.

When analyzing perturbations of the steady motion in order to check the system stability, all perturbed motions should be considered affected by different hysteretic coefficients $c_{hi} = h/|\omega_i - \omega|$, inversely proportional to their relative angular speed [10], but this approach would be scarcely productive for nonlinear systems with dry friction, like the present one. Therefore, when applying the small perturbation approach, very small deviations from the main deformation of the shaft will be assumed and the changes of the viscous-equivalent coefficient $c_h = h/\omega$ will be neglected in the calculation of the hysteretic force.

The amplitudes of the dry friction forces ϕ_3 and ϕ_4 are constant and their components in the xy -plane are given by $-\phi_jx'_j / \sqrt{x_j'^2 + y_j'^2}$ and $-\phi_jy'_j / \sqrt{x_j'^2 + y_j'^2}$ (for $j=3, 4$). If one or both supports are sticking, the sliding force ϕ_j must be replaced by the adhesive force $\phi_{adh,j}$, which must balance the other forces acting on the support.

All displacements are scaled by the rotor eccentricity e , all rotations by e/l , all forces by ke , and all moments by kel . Then, the dimensionless displacement-rotation vectors $\mathbf{X} = \{X_1, X_2, X_3, X_4\}^T$ and $\mathbf{Y} = \{Y_1, Y_2, Y_3, Y_4\}^T$ are introduced, where $X_j = x_j/e$, $Y_j = y_j/e$, for $j \neq 2$, and $X_j = \psi/l$, $Y_j = -\phi/l$, for $j=2$. The minus sign before the rotation ϕ is intentionally chosen in order to use the same stiffness and flexibility matrices on both the bending planes, xz and yz .

Considering all the forces and moments, the motion equations may be written in the form

$$\mathbf{KX} + 2\Omega\mathbf{DX}' + 2\mathbf{H}(\mathbf{X}' + \mathbf{Y}) + \Omega^2\mathbf{MX}'' + \Omega^2\mathbf{GY}' + \begin{pmatrix} -\Omega^2 \cos \theta \\ 0 \\ \frac{\sigma_3 \Phi_3 X'_3}{\sqrt{X_3'^2 + Y_3'^2}} + (1 - \sigma_3)\Phi_{adh,3,x} \\ \frac{\sigma_4 \Phi_4 X'_4}{\sqrt{X_4'^2 + Y_4'^2}} + (1 - \sigma_4)\Phi_{adh,4,x} \end{pmatrix} = 0$$

$$\mathbf{KY} + 2\Omega\mathbf{DY}' + 2\mathbf{H}(\mathbf{Y}' - \mathbf{X}) + \Omega^2\mathbf{MY}'' - \Omega^2\mathbf{GX}' + \begin{pmatrix} -\Omega^2 \sin \theta + \Gamma \\ 0 \\ \frac{\sigma_3 \Phi_3 Y_3}{\sqrt{X_3'^2 + Y_3'^2}} + (1 - \sigma_3)\Phi_{adh,3,y} + \Gamma M_3 \\ \frac{\sigma_4 \Phi_4 Y_4}{\sqrt{X_4'^2 + Y_4'^2}} + (1 - \sigma_4)\Phi_{adh,4,y} + \Gamma M_4 \end{pmatrix} = 0 \quad (1x,y)$$

where $\Phi_j = \phi_j/(ke)$, $\Phi_{adh,j} = \phi_{adh,j}/(ke)$, the numbers σ_j indicate the sliding ($\sigma_j=1$) or adhesive ($\sigma_j=0$) states of the dry friction surfaces, \mathbf{D} , \mathbf{M} , and \mathbf{G} are diagonal and are the damping, massive, and gyroscopic matrices, whose coefficients are (d_1, d_2, d_3, d_4) , $(1, J_a, M_3, M_4)$, and $(0, J_a, 0, 0)$ respectively, J_a and J_a being the dimensionless diametral and axial moment of inertia of the rotor. Moreover, \mathbf{K} and \mathbf{H} are the symmetric matrices of stiffness and hysteresis, and are given by

$$\mathbf{K} = \frac{1}{16L_3^3L_4^3} \begin{pmatrix} 1 - 3L_3L_4 & c_2L_3L_4(L_3 - L_4) & -L_4^3 & -L_3^3 \\ c_2L_3L_4(L_3 - L_4) & c_{22}L_3^2L_4^2 & c_2L_3L_4^3 & -c_2L_4L_3^3 \\ -L_4^3 & c_2L_3L_4^3 & 16L_3^3L_4^3K_3 + L_4^3 & 0 \\ -L_3^3 & -c_2L_4L_3^3 & 0 & 16L_3^3L_4^3K_4 + L_3^3 \end{pmatrix} \quad (2)$$

$$\mathbf{H} = d_h \begin{bmatrix} 1 & 0 & -L_4 & -L_3 \\ 0 & 0 & 0 & 0 \\ -L_4 & 0 & L_4^2 & L_3L_4 \\ -L_3 & 0 & L_3L_4 & L_3^2 \end{bmatrix} \tag{3}$$

where $c_2=c_{22}=1$ for a hinged–hinged shaft, while $c_2=1/2, c_{22}=1/3$ for a clamped–clamped shaft. Notice that for a cantilever shaft, for example clamped at the support 3 and carrying the rotor at the free end 4, all the above vectors and matrices become three-dimensional.

2.2. Equilibrium configuration and complex dynamical formulation

The constant part of the solution, i.e. the central equilibrium configuration of the rotor, can be easily obtained by Eq. (1), though this solution is not unique in theory in the case of adhesion between the friction surfaces. In fact, different vectors \mathbf{X}_{equil} and \mathbf{Y}_{equil} can be obtained by varying the adhesive force $\Phi_{adh,j}$, provided that the adhesion limit is not reached. Nevertheless, as the sliding/adhesive friction force must remain continuous in the sliding/adhesive transition when varying the rotor speed, the equilibrium position can be considered unique and is given by

$$\mathbf{X}_{equil} = 2\Gamma\mathbf{A}\mathbf{H}(\mathbf{K} + 4\mathbf{H}\mathbf{A}\mathbf{H})^{-1}\{1, 0, M_3, M_4\}^T, \quad \mathbf{Y}_{equil} = -\Gamma(\mathbf{K} + 4\mathbf{H}\mathbf{A}\mathbf{H})^{-1}\{1, 0, M_3, M_4\}^T \tag{4x,y}$$

where $\mathbf{A}=\mathbf{K}^{-1}$ is the flexibility matrix. Since $\mathbf{X}_{equil} \neq 0$, the well known static bias due to hysteresis is observable and, as the changes of \mathbf{Y}_{equil} consequent to hysteresis are small of order d_h^2 by Eq. (4y), while \mathbf{X}_{equil} is of order d_h by Eq. (4x), the hysteretic equilibrium position appears slightly displaced in the horizontal direction in the sense of the rotation. Anyway, in the following calculations, the vectors \mathbf{X} and \mathbf{Y} will be assumed deflated of their constant content (4) for simplicity, in order to focus better on the dynamical behaviour.

As the suspension stiffness is isotropic, all the system motions are circularly polarized and the dynamic part of Eqs. (1x,y) can be further compacted multiplying Eqs. (1y) by the unit imaginary number i , summing them to Eqs. (1x) and putting $\mathbf{W}=\mathbf{X}+i\mathbf{Y}, \hat{\Phi}_{adh,j} = \hat{\Phi}_{adh,j,x} + i\hat{\Phi}_{adh,j,y}$:

$$\mathbf{K}\mathbf{W} + 2\Omega\mathbf{D}\mathbf{W}' + 2\mathbf{H}(\mathbf{W}' - i\mathbf{W}) + \Omega^2\mathbf{M}\mathbf{W}'' - i\Omega^2\mathbf{G}\mathbf{W}' + \begin{Bmatrix} -\Omega^2 \exp(i\theta) \\ 0 \\ \sigma_3\Phi_3 \exp(i \arg W_3') + (1-\sigma_3)\hat{\Phi}_{adh,3} \\ \sigma_4\Phi_4 \exp(i \arg W_4') + (1-\sigma_4)\hat{\Phi}_{adh,4} \end{Bmatrix} = 0 \tag{5}$$

The uniqueness of the solution of Eq. (5) was proved in [6] in the absence of hysteresis ($d_h=0$) by assuming the existence of two different periodic solutions *ad absurdum* and ascertaining their necessary coincidence through an integration process over a common period. The stability of this solution was also proved defining a suitable positive-definite Lyapunov function. Nevertheless, in the presence of hysteresis the stability proof fails and unstable supercritical conditions may indeed arise.

2.3. Natural precession modes

The natural precession modes are to be considered in an ideal non-dissipative autonomous condition, where the matrices \mathbf{D} and \mathbf{H} vanish together with the gravitational-unbalance force vector. Using the complex notation $\mathbf{W}=\mathbf{W}_0 \exp(i\Omega_n\theta/\Omega)$, where $\Omega_n=\omega_n/\omega_c$ is a dimensionless precession speed and the subscript 0 denotes a constant amplitude vector, we get

$$[\mathbf{K} - \Omega_n^2(\mathbf{M} - \mathbf{G}\Omega/\Omega_n)\mathbf{W}_0 = \mathbf{Z}_0(\Omega, \Omega_n)\mathbf{W}_0 = 0 \rightarrow \det(\mathbf{Z}_0) = 0 \tag{6}$$

where the ideal dynamic matrix $\mathbf{Z}_0(\Omega, \Omega_n)$ is a function of the rotor speed and of the precession speed. Should we put $\mathbf{W}=\mathbf{X}-i\mathbf{Y}$ and subtract Eqs. (1y), multiplied by i , from Eqs. (1x), we would find the same precession equation, except for a plus sign in front of the gyroscopic term \mathbf{G} . Therefore, we would get opposite characteristic roots Ω_n with an opposite vector \mathbf{Y} , so that the natural whirling motions would be the same. Using the main notation $\mathbf{W}=\mathbf{X}+i\mathbf{Y}$, the precession motions turn out to be progressive or retrograde for $\Omega_n > 0$ or $\Omega_n < 0$ respectively, as can be deduced by calculating the dimensionless moment of the whirl velocity vector with respect to the z_0 axis of Fig. 1: $\{[(W_{0jr} \cos \beta - W_{0ji} \sin \beta)\mathbf{i}_x + (W_{0jr} \sin \beta + W_{0ji} \cos \beta)\mathbf{i}_y] \times [-\Omega_n(W_{0jr} \sin \beta + W_{0ji} \cos \beta)\mathbf{i}_x + \Omega_n(W_{0jr} \cos \beta - W_{0ji} \sin \beta)\mathbf{i}_y]\} \bullet \mathbf{i}_z = \Omega_n(W_{0jr}^2 + W_{0ji}^2)$, where W_{0jr} and W_{0ji} are the real and imaginary parts of $W_{0j}, \beta = \Omega_n\theta/\Omega$, and the \mathbf{i} 's are unit vectors. It is remarkable that in some special cases, for example with considerable anisotropy in the support stiffness, the precession of one of the supports or of the rotor axis may be counter-directed with respect to the rotor whirl for the same Ω_n (see [12]).

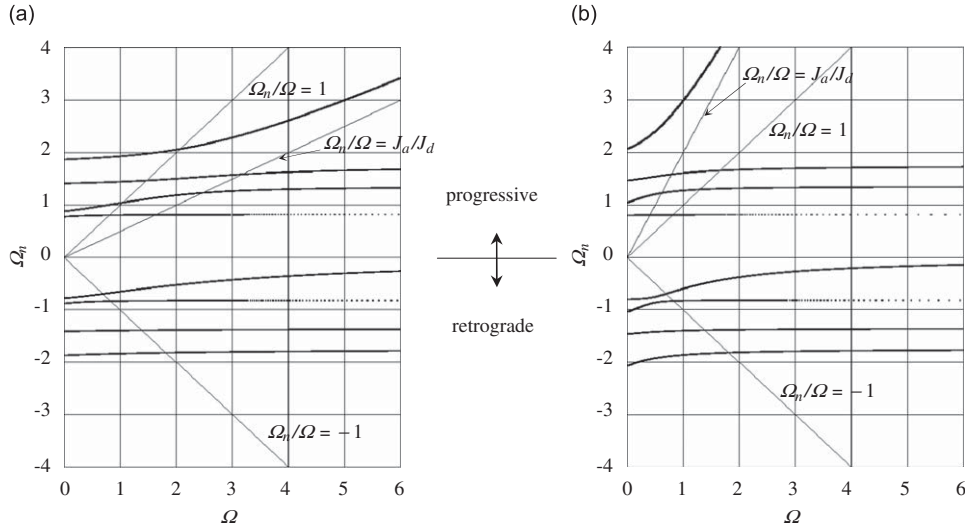


Fig. 2. Campbell diagrams $\Omega_n(\Omega)$ for $L_3 = 0.4, K_3 = K_4 = 1.5, M_3 = M_4 = 1$: (a) $J_a=0.1, J_d=0.2$ (oblong ellipsoid of inertia) and (b) $J_a=0.2, J_d=0.1$ (oblate ellipsoid of inertia).

Eq. (6) yields an eight degree characteristic polynomial in Ω_n , whose coefficients are functions of Ω . Putting $I=J_d-J_a\Omega/\Omega_n$ for brevity and indicating the cofactors with the superscript (c) , one gets $(K_{22}-I\Omega_n^2)Z_{0,22}^{(c)}+K_{12}Z_{0,12}^{(c)}+K_{32}Z_{0,32}^{(c)}+K_{42}Z_{0,42}^{(c)}=0$, i.e.

$$\begin{aligned} \Omega_n^8 - \left(K_{11} + \frac{K_{22}}{I} + \frac{K_{33}}{M_3} + \frac{K_{44}}{M_4} \right) \Omega_n^6 + \left(\frac{K_{33}K_{44}}{M_3M_4} + \frac{K_{22}K_{44}-K_{24}^2}{IM_4} + \frac{K_{22}K_{33}-K_{23}^2}{IM_3} + \frac{K_{11}K_{22}-K_{12}^2}{I} \right. \\ \left. + \frac{K_{11}K_{44}-K_{14}^2}{M_4} + \frac{K_{11}K_{33}-K_{13}^2}{M_3} \right) \Omega_n^4 - \left(\frac{K_{11}^{(c)}}{IM_3M_4} + \frac{K_{22}^{(c)}}{M_3M_4} + \frac{K_{33}^{(c)}}{IM_4} + \frac{K_{44}^{(c)}}{IM_3} \right) \Omega_n^2 + \frac{\det(\mathbf{K})}{IM_3M_4} = 0 \end{aligned} \quad (6b)$$

The roots of Eq. (6b) give the forward and backward precession speeds, for $\Omega_n > 0$ and $\Omega_n < 0$, respectively and can be traced on Campbell diagrams $\Omega_n(\Omega)$, symmetric with respect to the origin. Fig. 2 shows two example cases, for an oblong and an oblate ellipsoid of inertia of the rotor, and eight branches of the locus are visible on each diagram. The locus has an asymptote with slope J_a/J_d and seven other horizontal asymptotes, given by $\Omega_n=0$ and by the roots of the equation $Z_{0,22}^{(c)}=0$, which is cubic in Ω_n^2 . The critical angular speeds, $\Omega_n = \pm \Omega$, are identified by the intersection of the locus with the bisectors of the axes, where the minus sign refers to the critical retrograde precession (see Ref. [13]). Considering direct and retrograde precession motions altogether, we have eight or seven critical speeds for $J_a/J_d < 1$ or $J_a/J_d > 1$, respectively (oblong or oblate ellipsoid of inertia of the rotor).

3. Steady whirling motions

The steady circular solutions can be calculated putting $\mathbf{W}=\mathbf{W}_0 \exp(i\theta)$, where \mathbf{W}_0 is a complex amplitude vector. Observing that all hysteretic terms vanish, because the derivatives of \mathbf{W} are given by $\mathbf{W}^{(n)}=i^n \mathbf{W}$, Eq. (5) is transformable into

$$[\mathbf{K}+2i\Omega\mathbf{D}-\Omega^2(\mathbf{M}-\mathbf{G})]\mathbf{W}_0=(\mathbf{Z}_0+2i\Omega\mathbf{D})\mathbf{W}_0=\mathbf{Z}\mathbf{W}_0=\begin{Bmatrix} \Omega^2 \\ 0 \\ -i\sigma_3\Phi_3 \exp(i\arg W_{0,3})-(1-\sigma_3)\bar{\Phi}_{adh,3} \\ -i\sigma_4\Phi_4 \exp(i\arg W_{0,4})-(1-\sigma_4)\bar{\Phi}_{adh,4} \end{Bmatrix} \quad (7)$$

where \mathbf{Z} is the complex impedance matrix of the dynamical system, $\mathbf{Z}_0=\mathbf{Z}_0(\Omega, \Omega)$ is its real non-viscous part (see Eq. (6) in Section 2.3.), and the terms $-i\sigma_j\Phi_j$ and $-\bar{\Phi}_{adh,j}(1-\sigma_j)$ give the complex amplitudes of the sliding and adhesion forces.

The coefficients of the matrix \mathbf{Z} are real and symmetric in all the off-diagonal places, due to the diagonal nature of matrix \mathbf{D} , so that, indicating with i, j, k, l a generic combination without repetition of the subscripts 1, 2, 3, 4, the cofactors and the determinant of \mathbf{Z} can be separated into their real and imaginary parts:

$$\begin{aligned} Z_{ii}^{(c)} &= Z_{0,ii}^{(c)} - 4\Omega^2 \sum_{j \neq k \neq l} d_j d_k Z_{0,ll} + 2i\Omega \left[\sum_{j \neq k \neq l} d_j (Z_{0,kk} Z_{0,ll} - Z_{0,lk}^2) - 4\Omega^2 d_j d_k d_l \right] \\ z_{ij}^{(c)} &= Z_{0,ij}^{(c)} - 4\Omega^2 d_k d_l Z_{0,ij} - 2i\Omega [d_k (Z_{0,ij} Z_{0,ll} - Z_{0,il} Z_{0,jl}) + d_l (Z_{0,ij} Z_{0,kk} - Z_{0,ik} Z_{0,jk})] \\ \det(\mathbf{Z}) &= \det(\mathbf{Z}_0) - 4\Omega^2 \sum_{i \neq j \neq k \neq l} d_i d_j (Z_{0,kk} Z_{0,ll} - Z_{0,kl}^2) + 16\Omega^4 d_1 d_2 d_3 d_4 + 2i\Omega \left[\sum_i d_i Z_{0,ii}^{(c)} - 4\Omega^2 \sum_{i \neq j \neq k \neq l} d_i d_j d_k Z_{0,ll} \right] \end{aligned} \quad (8)$$

Then, carrying out the inversion of the matrix \mathbf{Z} , $\mathbf{Z}^{-1} = [\mathbf{Z}_{ij}^{(c)}]^\top / \det(\mathbf{Z})$, it is possible to solve for \mathbf{W}_0 , i.e. $\mathbf{W}_0 = \mathbf{Z}^{-1} \{\Omega^2, 0, -i\sigma_3 \Phi_3 \exp(i \arg W_{0,3}) - (1 - \sigma_3) \hat{\Phi}_{adh,3}, -i\sigma_4 \Phi_4 \exp(i \arg W_{0,4}) - (1 - \sigma_4) \hat{\Phi}_{adh,4}\}^\top$ and calculate the moduli R_j and the arguments γ_j of its components $W_{0,j} = R_j \exp(-i\gamma_j)$. Here the R_j are the orbital radii of the rotor and the supports for $j \neq 2$, while R_2 is the angular amplitude of the rotor axis cone. If there is adhesion between the friction surfaces of any one of the two supports ($\sigma_j = 0$), the sliding term $-i\Phi_j \exp(-i\gamma_j)$ must be replaced by the adhesive term $-\hat{\Phi}_{adh,j}$, with unknown argument and modulus. Nevertheless, the addition of an extra unknown is compensated by the vanishing of the radius R_j . More generally, it is convenient to replace the exponential term $\exp(-i\gamma_j)$ with a complex friction number \hat{N}_j , whose modulus and argument are 1 and $-\gamma_j$ for $R_j > 0$, but are both unknown for $R_j = 0$, in which case $|\hat{N}_j|$ becomes equal to the ratio of the adhesive force to the sliding force.

The solution can be written down in the form

$$\begin{aligned} R_1 \exp(-i\gamma_1) &= c_{10} - ic_{13} \hat{N}_3 - ic_{14} \hat{N}_4 \\ R_2 \exp(-i\gamma_2) &= c_{20} - ic_{23} \hat{N}_3 - ic_{24} \hat{N}_4 \\ R_3 \exp(-i\gamma_3) &= c_{30} - ic_{33} \hat{N}_3 - ic_{34} \hat{N}_4 \\ R_4 \exp(-i\gamma_4) &= c_{40} - ic_{43} \hat{N}_3 - ic_{44} \hat{N}_4 \end{aligned} \tag{9a-d}$$

where the coefficients $c_{ij} = c_{ij,r} + ic_{ij,i}$ are complex in general, but become real in the absence of viscous dissipation ($c_{ij,i} = 0$ for $\mathbf{D} \equiv 0$).

Fixing the rotor angular speed, the solution procedure is similar to [6], as summarised hereafter. Assuming firstly sliding conditions for both the journal boxes, one puts $\hat{N}_j = \exp(-i\gamma_j)$ and solves Eqs. (9) for the eight quantities R_j and γ_j . If no couple of real positive roots can be found for R_3 and R_4 , one or both the journal boxes are stuck and new solutions are sought in the hypothesis of adhesion of the one or the other support. Therefore, one puts either $R_3 = 0$ or $R_4 = 0$ and calculates the correspondent complex number, \hat{N}_3 or \hat{N}_4 , together with the orbital radius, R_4 or R_3 , of the other sliding support. If a positive radius of any one of the two supports cannot yet be found when the other is assumed stuck, there are stick conditions on both of them and the numbers \hat{N}_j are calculated by putting $R_3 = R_4 = 0$. It must be said that, if two possible whirling motions happen to be found, the one with sticking/sliding conditions of the supports 3/4, and the other of the supports 4/3, the solution giving a continuous transition from the sliding to the stick state has to be chosen.

Furthermore, on the basis of the above procedure, an optimization process may be carried out for the mechanical characteristics of the support system and for the level of the dry friction forces, in order to minimize the whirling motions in the most proper manner. In practice, fixing the system parameters and some specific weights for the orbital

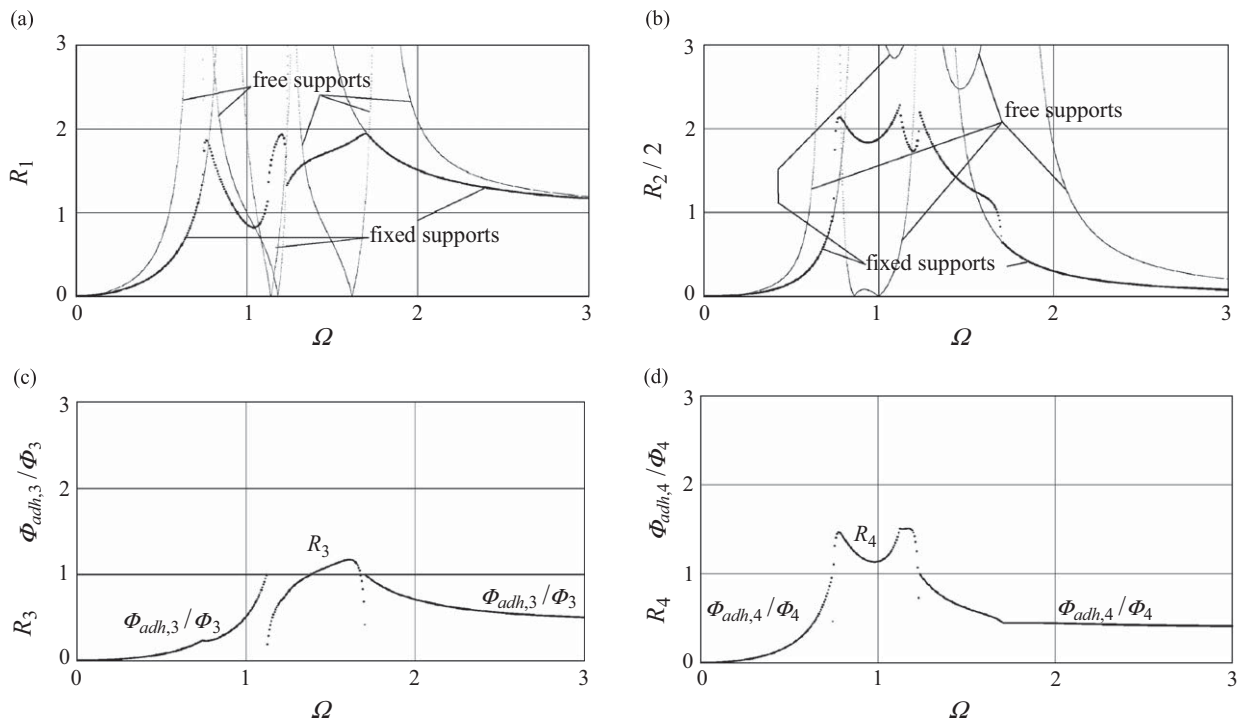


Fig. 3. (a)–(d) Optimized frequency response for hinged-hinged rotor–shaft system. Data: $\Phi_3 = 2.4054688$, $\Phi_4 = 0.746875$, $w_1 = w_2 = 0.3$, $w_3 = w_4 = 0.2$, $L_3 = 0.4$, $d_1 = d_2 = d_3 = d_4 = 0$, $d_h = 0.05$, $K_3 = K_4 = 1$, $M_3 = M_4 = 1$, $J_d = 0.4$, $J_a = 0.2$.

amplitudes of the rotor and the supports, the optimization may aim at minimizing the maximum value of their weighted average throughout the speed range by varying the dry friction level. The optimization process may be carried out numerically, varying the two parameters Φ_3 and Φ_4 gradually, spanning the speed range at each step, estimating the maximum weighted average of the orbital radii, and reducing the step size when this average approaches a minimum value.

Figs. 3a–d show the optimized speed responses of the rotor (R_1, R_2) and the supports (R_3, R_4) for an example case with a hinged–hinged shaft and no viscous damping. The rotor response in the two cases of fixed–fixed and floating–floating journal boxes are also shown (i.e. for $\Phi_j \rightarrow \infty$ and $\Phi_j \rightarrow 0$, respectively). It is possible to appreciate the good efficiency of the dry friction dampers in cutting all critical speeds, by either getting into or getting off the adhesive state, and in restraining the whirl amplitude in the remaining range. Figs. 3c and d show also the adhesive force level in the stuck range.

The dry friction damper behaviour is thus similar to that of automatic clutches controlled by the shaft speed, which block the journal boxes when some critical speed of the floating–support system is expected and release them when the critical speeds of the fixed–support configuration are being approached.

4. Nonlinear stability

The stability of the steady motion can be tested by the small perturbation approach, assuming that a small perturbation, consisting of the vectors $\tilde{\mathbf{X}}$ and $\tilde{\mathbf{Y}}$, is superimposed on the steady solution, here indicated without any over-sign. One gets by Eqs. (9), for full sliding of both supports,

$$\mathbf{K}\tilde{\mathbf{X}} + 2\Omega\mathbf{D}\tilde{\mathbf{X}}' + 2\mathbf{H}(\tilde{\mathbf{X}}' + \tilde{\mathbf{Y}}) + \Omega^2(\mathbf{M}\tilde{\mathbf{X}}'' + \mathbf{G}\tilde{\mathbf{Y}}') + \left\{ \begin{array}{l} 0 \\ 0 \\ \Phi_3 \left[\frac{X_3 + \tilde{X}_3}{\sqrt{(X_3 + \tilde{X}_3)^2 + (Y_3 + \tilde{Y}_3)^2}} - \frac{X_3}{\sqrt{X_3^2 + Y_3^2}} \right] \\ \Phi_4 \left[\frac{X_4 + \tilde{X}_4}{\sqrt{(X_4 + \tilde{X}_4)^2 + (Y_4 + \tilde{Y}_4)^2}} - \frac{X_4}{\sqrt{X_4^2 + Y_4^2}} \right] \end{array} \right\} = 0 \quad (10x)$$

$$\mathbf{K}\tilde{\mathbf{Y}} + 2\Omega\mathbf{D}\tilde{\mathbf{Y}}' + 2\mathbf{H}(\tilde{\mathbf{Y}}' - \tilde{\mathbf{X}}) + \Omega^2(\mathbf{M}\tilde{\mathbf{Y}}'' - \mathbf{G}\tilde{\mathbf{X}}') + \left\{ \begin{array}{l} 0 \\ 0 \\ \Phi_3 \left[\frac{Y_3 + \tilde{Y}_3}{\sqrt{(X_3 + \tilde{X}_3)^2 + (Y_3 + \tilde{Y}_3)^2}} - \frac{Y_3}{\sqrt{X_3^2 + Y_3^2}} \right] \\ \Phi_4 \left[\frac{Y_4 + \tilde{Y}_4}{\sqrt{(X_4 + \tilde{X}_4)^2 + (Y_4 + \tilde{Y}_4)^2}} - \frac{Y_4}{\sqrt{X_4^2 + Y_4^2}} \right] \end{array} \right\} = 0 \quad (10y)$$

If one of the supports happens to be motionless in stuck conditions, the correspondent static friction term is unknown, but the orbital amplitude vanishes and the mathematical problem remains consistent. If both journal boxes are blocked, the system becomes linear and the stability may be controlled by the conventional Routh–Hurwitz procedure.

As we are just considering small perturbations, the nonlinear friction terms of Eqs. (10) may be approximated by the linear expressions:

$$\Phi_j \frac{Y_j (Y_j \tilde{X}_j' - X_j \tilde{Y}_j')}{(X_j^2 + Y_j^2) \sqrt{X_j^2 + Y_j^2}} \text{ in (10x)} \quad \text{and} \quad \Phi_j \frac{X_j (X_j \tilde{Y}_j' - Y_j \tilde{X}_j')}{(X_j^2 + Y_j^2) \sqrt{X_j^2 + Y_j^2}} \text{ in (10y)}$$

where considering the results of the previous section, X_j and Y_j are the real and imaginary parts of W_j . The 4+4 equations of the differential system (10x,y) can be transformed into the following canonical form, where some coefficients are variable and π -periodic:

$$\begin{aligned} \tilde{\mathbf{X}}' &= \tilde{\mathbf{U}} \\ \tilde{\mathbf{Y}}' &= \tilde{\mathbf{V}} \\ \tilde{\mathbf{U}}' &= -\frac{\mathbf{M}^{-1}}{\Omega^2} \left[\mathbf{K}\tilde{\mathbf{X}} + 2\Omega\mathbf{D}\tilde{\mathbf{U}} + 2\mathbf{H}(\tilde{\mathbf{U}} + \tilde{\mathbf{V}}) + \Omega^2\mathbf{G}\tilde{\mathbf{V}} + \left\{ \begin{array}{l} 0 \\ 0 \\ \frac{\Phi_3}{R_3} [\tilde{U}_3 \cos^2(\theta - \gamma_3) + \tilde{V}_3 \sin(\theta - \gamma_3) \cos(\theta - \gamma_3)] \\ \frac{\Phi_4}{R_4} [\tilde{U}_4 \cos^2(\theta - \gamma_4) + \tilde{V}_4 \sin(\theta - \gamma_4) \cos(\theta - \gamma_4)] \end{array} \right\} \right] \end{aligned}$$

$$\tilde{\mathbf{V}}' = -\frac{\mathbf{M}^{-1}}{\Omega^2} \left[\mathbf{K}\tilde{\mathbf{Y}} + 2\Omega\mathbf{D}\tilde{\mathbf{V}} + 2\mathbf{H}(\tilde{\mathbf{U}} - \tilde{\mathbf{X}}) - \Omega^2\mathbf{G}\tilde{\mathbf{U}} + \begin{pmatrix} 0 \\ 0 \\ \frac{\Phi_3}{R_3} [\tilde{V}_3 \sin^2(\theta - \gamma_3) + \tilde{U}_3 \sin(\theta - \gamma_3) \cos(\theta - \gamma_3)] \\ \frac{\Phi_4}{R_4} [\tilde{V}_4 \sin^2(\theta - \gamma_4) + \tilde{U}_4 \sin(\theta - \gamma_4) \cos(\theta - \gamma_4)] \end{pmatrix} \right] \quad (11)$$

Due to the periodicity of the coefficients, the Floquet theory must be applied to ascertain the stable or unstable nature of the perturbed motion [14]. For this purpose, one has to firstly calculate the 16×16 fundamental matrix solution $\Theta(\theta)$, so that $\Theta(0)$ is equal to the identity matrix \mathbf{I} , and this task can be fulfilled by some routine of the Euler–Cauchy or Runge–Kutta type. Then, the characteristic multipliers must be extracted, i.e. the eigenvalues of $\Theta(\theta)$ after one period π , through the 16th degree algebraic characteristic equation $E_c(\lambda) = \det[\Theta(\pi) - \lambda\mathbf{I}] = \lambda^{16} + b_1\lambda^{15} + \dots + b_{15}\lambda + b_{16} = 0$. Stability requires all the characteristic multipliers to be smaller than one in modulus.

If one support, say j , is stuck to the frame due to an adhesive state of its friction surfaces, all the terms of the correspondent rows ($X_j \rightarrow, Y_j \rightarrow, U_j \rightarrow, V_j \rightarrow$) and columns ($X_j \downarrow, Y_j \downarrow, U_j \downarrow, V_j \downarrow$) of $\Theta(\pi)$ are replaced by zeroes, so that a factor λ^4 arises artificially in the characteristic equation, $E_c(\lambda) = \lambda^4(\lambda^{12} + b_1\lambda^{11} + \dots)$. This factor is uninfluential on the system stability as point $\lambda=0$ is just the centre at the unitary circle in the Argand plane. If both supports are stuck, the differential system reduces to the constant coefficient form and the Routh–Hurwitz criterion is sufficient to check the system stability. All these occurrences can be automatically controlled by the computational procedure.

The coefficients b_j of the characteristic polynomial E_c can be calculated by a collocation-type method, on obtaining the matrix $\Theta_\pi = \Theta(\pi)$. The first and last coefficients, $b_1 = -\text{Tr}(\Theta_\pi)$ and $b_{16} = \det(\Theta_\pi)$, are firstly calculated and then the other 14 b_j are obtainable by choosing 7 distinct numbers n , e.g. $n=1, 2, 3, 4, 5, 6, 7$, and writing

$$b_2n^{14} + b_3n^{13} + \dots + b_{14}n^2 + b_{15}n = -\det(\Theta_\pi) + \text{Tr}(\Theta_\pi)n^{15} - n^{16} + E_c(n) \quad (12a)$$

$$b_2n^{14} - b_3n^{13} + \dots + b_{14}n^2 - b_{15}n = -\det(\Theta_\pi) - \text{Tr}(\Theta_\pi)n^{15} - n^{16} + E_c(-n) \quad (12b)$$

Summing and subtracting the 7+7 equations, Eqs. (12), one gets two algebraic systems, for the even and odd coefficients separately:

$$b_2n^{14} + b_4n^{12} + \dots + b_{14}n^2 = -\det(\Theta_\pi) - n^{16} + \frac{E_c(n) + E_c(-n)}{2} \quad (13a)$$

$$b_3n^{13} + b_5n^{11} + \dots + b_{15}n = \text{Tr}(\Theta_\pi)n^{15} + \frac{E_c(n) - E_c(-n)}{2} \quad (13b)$$

where the right hands are to be considered as known terms because the determinants $E_c(n)$ and $E_c(-n)$ are easily calculable by common numerical routines.

Actually, on obtaining the polynomial $E_c(\lambda)$, there is no practical need to calculate its roots, but it is sufficient to verify that they lie inside the unit circle of the complex plane of Gauss–Argand, taking into account that $E_c(\lambda) = (\lambda - \lambda_1)(\lambda - \lambda_2)(\lambda - \lambda_3)\dots(\lambda - \lambda_{16})$ can be thought of as the product of 16 complex vectors $(\lambda - \lambda_j)$. Letting the variable λ move counter-clockwise along the unit circle, where $\lambda = \exp(i\phi)$, starting from the real axis ($\phi=0$) and reaching the starting position again at the end of one complete turn ($\phi=2\pi$), the argument of its “conformal image” $E_c(i\phi)$ changes by 16 times 2π if all the roots λ_j remain on the left of this path; otherwise it performs a lesser number of turns when some roots lie outside the unit circle. Relying on these considerations, the numerical check of stability requires just a short time on a common PC and moreover, the process may be re-iterated, changing some mechanical characteristic, for example until the stability threshold is identified.

As an example, Figs. 4a and b refer to the optimized rotor-shaft system described by Fig. 3. The viscous damping level needed to assure stable rotating motion is shown in Fig. 4a, together with the steady responses of the supports and their changes with respect to the undamped system. The corresponding steady response of the rotor and its changes due to the damping are shown in Fig. 4b. The undamped response is represented by thin lines in Figs. 4a and b. Only small changes of the response curves can be observed, so that the undamped steady analysis of Section 3 can be applied with a sufficient approximation also for small damping levels. The value of the viscous damping factor is assumed identical for the rotor and the supports (d) and is here scaled by the hysteresis factor d_h . The thin curve d/d_h of Fig. 4a refers to the fixed support configuration and points out that some viscous damping is needed above the first critical speed. As observable, just a small amount of damping is required, but this amount is largely reduced on average in the sliding range of the supports, due to the dry friction dissipation.

Figs. 5a and b show diagrams analogous to Fig. 4, but for a non-optimized system with a quite larger dry friction level. The sliding ranges of the journal boxes are much narrower and are in the close neighbourhood of critical speeds of the fixed support system. The rotor response exhibits larger orbital radii on average, in comparison with the optimized case of Fig. 4,

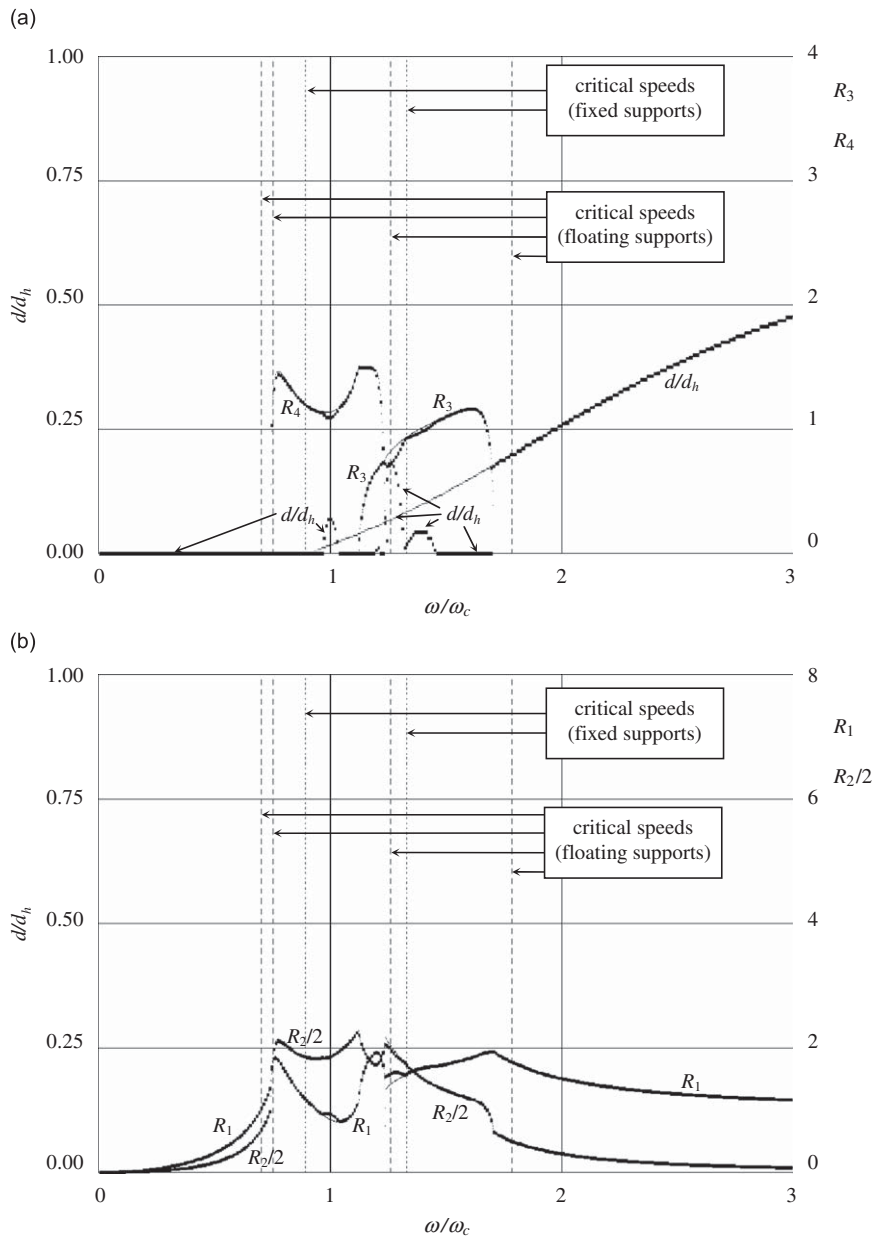


Fig. 4. (a, b) Viscous damping at stability threshold: $d_h=0.05$, $d_1=d_2=d_3=d_4=d$, Other data as in Fig. 3, i.e. $\Phi_3=2.4054688$, $\Phi_4=0.746875$ $w_1=w_2=0.3$, $w_3=w_4=0.2$, $L_3=0.4$, $K_3=K_4=1$, $M_3=M_4=1$, $J_d=0.4$, $J_a=0.2$.

and no practical advantage is likely to be expected with regard to the stabilization of the hysteretic whirl, as the high speed range provides stuck conditions for both cases.

On the contrary, Figs. 6a and b consider the case of lower dry friction forces, where more prominent resonance peaks can be observed. Nevertheless, the hysteretic whirl instability is well counteracted by the sliding state of the dry friction surface in the supercritical range.

Comparing Figs. 4–6, it is possible to see that the best restriction of the steady amplitude can be obtained on average by the optimization process, where the orbital radius and the half-conicity reach roughly the value 2 at most (Fig. 4b). A higher friction level eliminates the critical speeds as well, but gives higher resonant peaks (Fig. 5). On the contrary, a lower level may maintain the supports always in sliding conditions, to the advantage of stability, but cannot cut the critical speeds of the floating support configuration (Fig. 6).

The sliding or stuck conditions of the supports in the high speed range can be easily detected by the formulas of Section 3. Assuming dissipation only due to dry friction and considering the dominant terms of the impedance matrix \mathbf{Z}_0 of

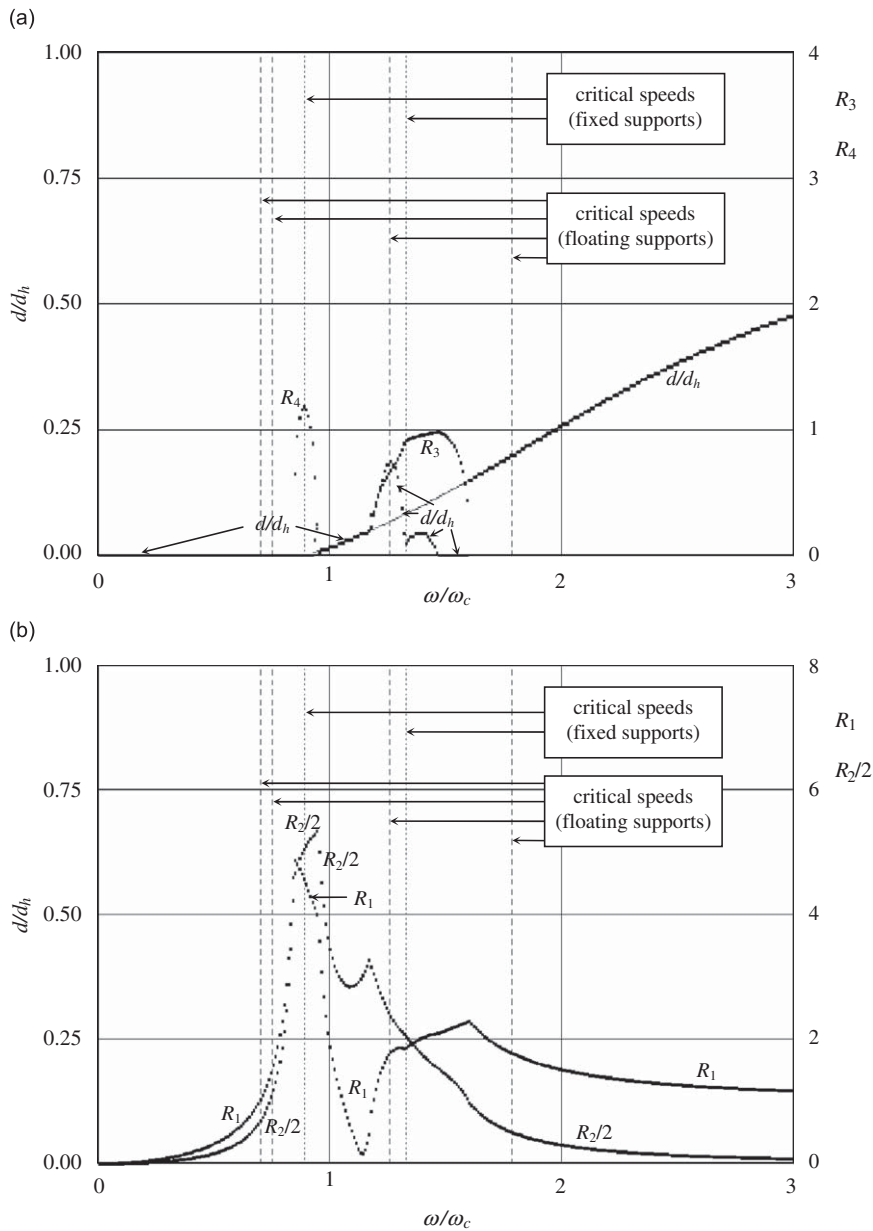


Fig. 5. (a, b) Viscous damping at stability threshold: $d_h=0.05$, $d_1=d_2=d_3=d_4=d$, Data: $\Phi_3=3$, $\Phi_4=3$, $w_1=w_2=0.3$, $w_3=w_4=0.2$, $L_3=0.4$, $K_3=K_4=1$, $M_3=M_4=1$, $J_d=0.4$, $J_a=0.2$.

Eq. (7) for $\Omega \rightarrow \infty$, Eqs. (9c,d) can be found to reduce to the simple form

$$R_3 \exp(-i\gamma_3) = \frac{-K_{31} + i\Phi_3 \hat{N}_3 + i\Phi_4 \hat{N}_3 \left[\frac{K_{31}K_{14}(J_d - J_a) + K_{32}K_{24}}{M_4(J_d - J_a)} \right]}{M_3(J_d - J_a)}$$

$$R_4 \exp(-i\gamma_4) = \frac{-K_{41} + i\Phi_3 \hat{N}_3 \left[\frac{K_{41}K_{13}(J_d - J_a) + K_{42}K_{23}}{M_4(J_d - J_a)} \right] + i\Phi_4 \hat{N}_4}{M_4(J_d - J_a)} \quad (14a,b)$$

Proceeding as in Section 3, it is possible to find that the sliding conditions of the one or the other support, or the simultaneous sliding of both of them, imply

$$R_j^2 = \frac{1 - (16L_j^3 \Phi_j)^2}{(16L_j^3 M_j \Omega^2)^2} \quad (15)$$

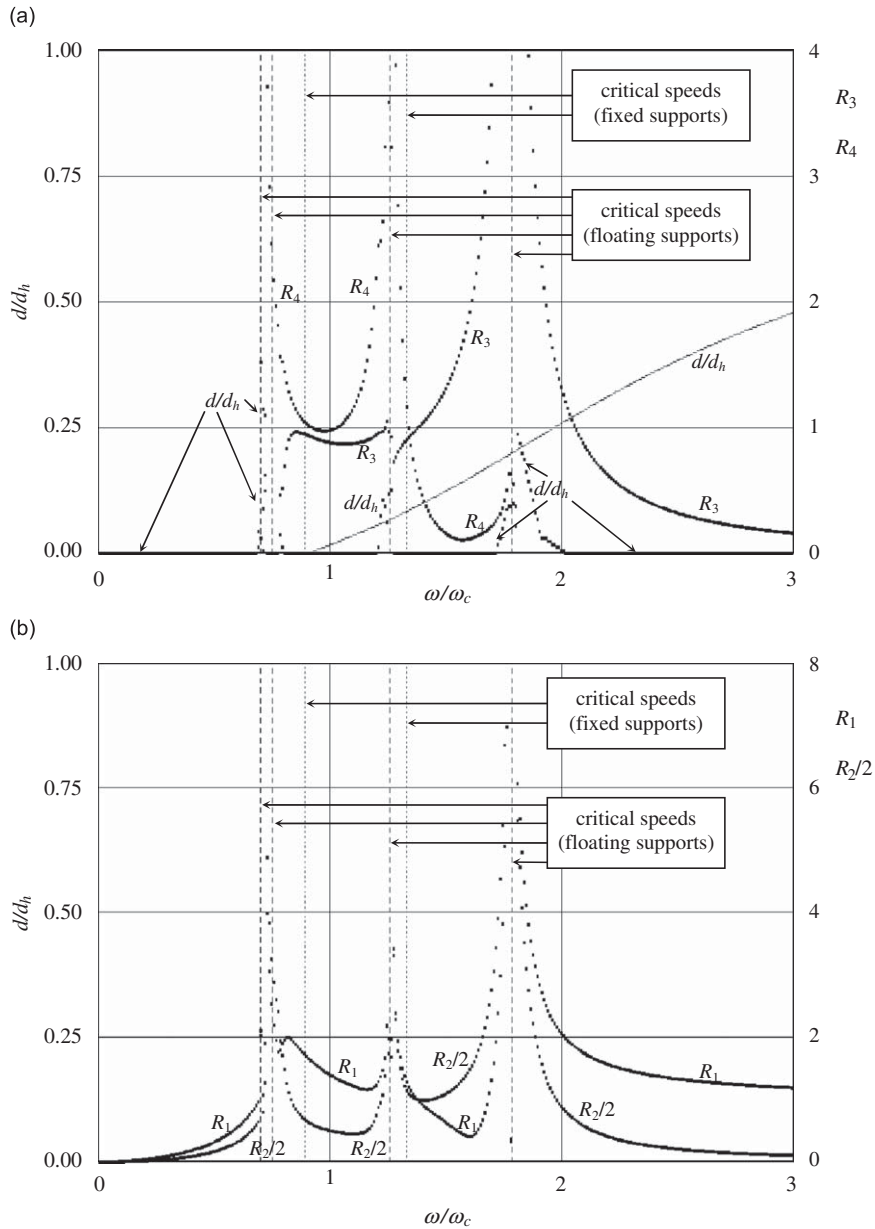


Fig. 6. (a, b) Viscous damping at stability threshold: $d_h=0.05$, $d_1=d_2=d_3=d_4=d$, Data: $\Phi_3=0.5$, $\Phi_4=0.5$ $w_1=w_2=0.3$, $w_3=w_4=0.2$, $L_3=0.4$, $K_3=K_4=1$, $M_3=M_4=1$, $J_d=0.4$, $J_a=0.2$.

whence $R_j \neq 0$ for $\Omega \rightarrow \infty$ only if $16L_j^3 \Phi_j < 1$. Clearly, for $\Phi_3 = \Phi_4$, the support farther from the rotor is the first one that will stick to the frame on increasing the dry friction level. Then, if $L_3 < 1/2$, the dry friction stabilization of the supercritical hysteretic whirl can be obtained if at least $\Phi_3 < 1/(16L_3^3)$. Nevertheless, it is to be recalled that the supercritical operation with sliding surfaces is somehow detrimental in terms of power dissipation and wear, so that an overall comparative analysis with the viscous damping should be advisable.

At this point an important consideration is appropriate. As the above approach refers to just small perturbation of the main motion and considers only linear stability, nothing can be concluded about nonlinear stability, where the effects of the dry friction forces become relevant. Moreover, in the case of sticking supports, the instability of the steady motion leads necessarily to release the adhesive contact between the friction surfaces and the arising sliding forces have a strong stabilising influence.

The nonlinear stability can be properly inspected by the direct numerical solution of the differential system, for example by some Runge–Kutta routine, starting from random initial conditions and proceeding as far as a large number of cycles are completed (100 or more). In this manner, the important result is obtainable that the unstable whirling motion does not lead at all to divergent conditions, as could be predicted by the linear analysis, but simply to a sort of small

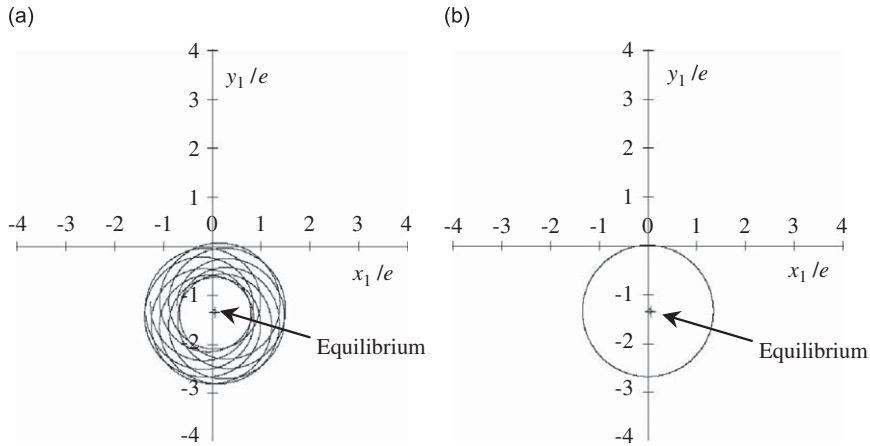


Fig. 7. (a) Non-periodic rotor centre path for a linearly unstable configuration. $K_3=K_4=M_3=M_4=0.2, J_d=0.4, J_a=0.2, d_h=0.1, d_1=d_2=d_3=d_4=0.25d_h, \omega/\omega_c=4, L_3=0.4, \Gamma=0.3, \Phi_3=1.3160156, \Phi_4=0.39335938$ (interval: 20 cycles). (b) Periodic rotor centre path for a linearly stable configuration. $K_3=K_4=M_3=M_4=0.2, J_d=0.4, J_a=0.2, d_h=0.1, d_1=d_2=d_3=d_4=0.25d_h, \omega/\omega_c=2, L_3=0.4, \Gamma=0.3, \Phi_3=1.3160156, \Phi_4=0.39335938$ (interval: 20 cycles).

wobbling of the trajectories in the very close neighbourhood of their steady circular attractors. This asymptotic behaviour is clearly visible in Fig. 7a, which refers to an unstable linear solution, while Fig. 7b shows the steady state reached after a large number of turns, starting from stable initial condition.

Summing up, the dry friction dampers are found to exert a very important quenching effect on the small unstable motions that may arise throughout the speed range, in the sense that these motions are limited to a very small wandering of the trajectories in the close neighbourhood of the steady circular paths. Nevertheless, as pointed out above, if the operative conditions of the rotor-shaft-support system are planned for the adhesive supercritical regime, such trembling motion of the support might not be convenient, due to the increase of wear and heat production. It should be checked if it is better to achieve the stabilization by other external dissipative sources—a comparison between the two form of dissipation, dry and viscous, can suggest the solution to be preferred.

5. Stabilization by viscous dampers

The product $c_h\omega$ has been assumed constant in the previous analysis because the main straining motion of the shaft is a rotation with speed $-\omega$ of the equilibrium deflection plane relative to the rotating frame $O_3\xi_0\eta_0\zeta_0$. Therefore, making the hypothesis of very small changes of the shaft deflection line, the hysteresis coefficient c_h has been assumed independent of the perturbation.

In the case of a vertical shaft on the contrary, or when the rotor weight is negligible with respect to the elastic and inertia force ($\Gamma \ll 1$), or when the perturbations are large, all natural whirling modes arise spontaneously with their own precession speeds and, following [10], different hysteretic coefficients must be taken into consideration. These coefficients must be assumed inversely proportional to the angular relative speed with respect to the frame $O_3\xi_0\eta_0\zeta_0$ and must be written in the form $c_h=h/|\omega_n-\omega|$, where ω_n indicates the absolute speed of any single precession. Though this new model complicates the analysis of the system stability enormously, a linear approach may lead to very interesting results for a suspension system subject only to viscous dissipation and not to dry friction. Moreover, as reported in Ref. [12], the stability analysis can be extended to cases with anisotropic suspension systems, with different stiffness characteristics in the two deflection planes of the shaft, by a proper modification of the system equations.

As the system is linear in the absence of dry friction, Eq. (5) applies also to the perturbed motions after cancelling the unbalance terms and replacing d_h with $h/(2k|\Omega_n-\Omega-1|)$ in Eq. (3). Putting $\mathbf{W}=\mathbf{W}_0 \exp(i\theta\tilde{\Omega}/\Omega)$, where \mathbf{W}_0 is a constant vector and $\tilde{\Omega}=\tilde{\omega}/\omega_c$ denotes one of the perturbation characteristic numbers, Eq. (5) can be written in the form

$$\left[\mathbf{K} + 2i\tilde{\Omega}\mathbf{D} + 2i\mathbf{H} \frac{\left(\frac{\tilde{\Omega}}{\Omega} - 1\right)}{\left|\frac{\Omega_n}{\Omega} - 1\right|} - \tilde{\Omega}^2 \left(\mathbf{M} - \mathbf{G} \frac{\Omega}{\tilde{\Omega}}\right) \right] \mathbf{W}_0 = \mathbf{Z}\mathbf{W}_0 = 0 \tag{16}$$

which still permits ascribing the scalar factor $d_h=0.5h/k$ to the matrix \mathbf{H} , as in Eq. (3).

The perturbed precession modes are obtainable by equating to zero the determinant of Eq. (16) and turn out to be stable if the imaginary part of $\tilde{\Omega}$ is positive. For $\mathbf{D}=\mathbf{H}=0$, these speeds would be equal to the previous natural speeds in Section 2.3, $\tilde{\Omega}=\Omega_n$, progressive for $\Omega_n > 0$ or retrograde for $\Omega_n < 0$. In the presence of dissipation on the contrary, the search for the characteristic numbers is just tricky, but simple approximate solutions can be obtained through the hypothesis that the viscous and hysteretic factors are quite small, as generally occurs in all practical situations, so that the dissipative precession speeds differ very little from the non-dissipative ideal system. Assuming then $d_h (\ll 1)$ as a small reference parameter, one may put $\tilde{\Omega}=\Omega_n+d_h\lambda, d_j=d_h\delta_j$, where λ and δ_j are of order one.

Neglecting terms of order d_h^2 , the matrix \mathbf{Z} of Eq. (16) changes to

$$\mathbf{Z} \cong \begin{bmatrix} K_{11} + 2id_h \left[\delta_1 \Omega_n + \operatorname{sgn} \left(\frac{\Omega_n}{\Omega} - 1 \right) \right] - \Omega_n^2 \left(1 + \frac{2d_h \lambda}{\Omega_n} \right) & K_{12} \\ K_{21} & K_{22} + 2id_h \delta_2 \Omega_n - J_d \Omega_n^2 \left(1 + \frac{2d_h \lambda}{\Omega_n} \right) + \Omega \Omega_n J_a \left(1 + \frac{d_h \lambda}{\Omega_n} \right) \\ K_{31} - 2d_h L_4 \operatorname{sgn} \left(\frac{\Omega_n}{\Omega} - 1 \right) & K_{32} \\ K_{41} - 2d_h L_3 \operatorname{sgn} \left(\frac{\Omega_n}{\Omega} - 1 \right) & K_{42} \\ K_{13} - 2d_h L_4 \operatorname{sgn} \left(\frac{\Omega_n}{\Omega} - 1 \right) & K_{14} - 2d_h L_3 \operatorname{sgn} \left(\frac{\Omega_n}{\Omega} - 1 \right) \\ K_{23} & K_{24} \\ K_{33} + 2id_h \left[\delta_3 \Omega_n + L_4^2 \operatorname{sgn} \left(\frac{\Omega_n}{\Omega} - 1 \right) \right] - M_3 \Omega_n^2 \left(1 + \frac{2d_h \lambda}{\Omega_n} \right) & 2d_h L_3 L_4 \operatorname{sgn} \left(\frac{\Omega_n}{\Omega} - 1 \right) \\ 2d_h L_3 L_4 \operatorname{sgn} \left(\frac{\Omega_n}{\Omega} - 1 \right) & K_{44} + 2id_h \left[\delta_4 \Omega_n + L_3^2 \operatorname{sgn} \left(\frac{\Omega_n}{\Omega} - 1 \right) \right] - M_4 \Omega_n^2 \left(1 + \frac{2d_h \lambda}{\Omega_n} \right) \end{bmatrix} \quad (17)$$

Eq. (17) appears in the form $\mathbf{Z} = \mathbf{Z}_0 + d_h \mathbf{Z}_1$, where \mathbf{Z}_0 is the same as in Section 2.3 and its determinant is zero because the numbers Ω_n refer to the ideal whirling modes.

Continuing the neglect of all terms of order d_h^2 or higher, the vanishing of $\det(\mathbf{Z})$ implies in practice equating to zero the sum of the products of the single terms of \mathbf{Z}_1 with their correspondent cofactors in the matrix \mathbf{Z}_0 , which are here indicated by $Z_{0,ij}^{(c)}$. Therefore

$$i\lambda \Omega_n \left[Z_{0,11}^{(c)} + Z_{0,22}^{(c)} \left(J_d - \frac{\Omega}{2\Omega_n} J_a \right) + Z_{0,33}^{(c)} M_3 + Z_{0,44}^{(c)} M_4 \right] + \Omega_n \left[Z_{0,11}^{(c)} \delta_1 + Z_{0,22}^{(c)} \delta_2 + Z_{0,33}^{(c)} \delta_3 + Z_{0,44}^{(c)} \delta_4 \right] + \operatorname{sgn} \left(\frac{\Omega_n}{\Omega} - 1 \right) \left[Z_{0,11}^{(c)} + 2L_3 L_4 Z_{0,34}^{(c)} + Z_{0,33}^{(c)} L_4^2 + Z_{0,44}^{(c)} L_3^2 - 2(Z_{0,13}^{(c)} L_4 + Z_{0,14}^{(c)} L_3) \right] = 0 \quad (18)$$

Here λ appears to be a pure imaginary number to a first approximation, so that the real quantity $i\lambda$ must be negative for whirling motion stability. Moreover, an important though expected result is that the stability of precession motion strongly depends on whether the rotor speed Ω is higher or lower than the natural speed Ω_n .

As an example, Fig. 8 shows the results obtainable by Eq. (18) for each of the eight precession motions. The equality of all viscous damping factors was supposed in the analysis and the stability threshold was defined as the minimum

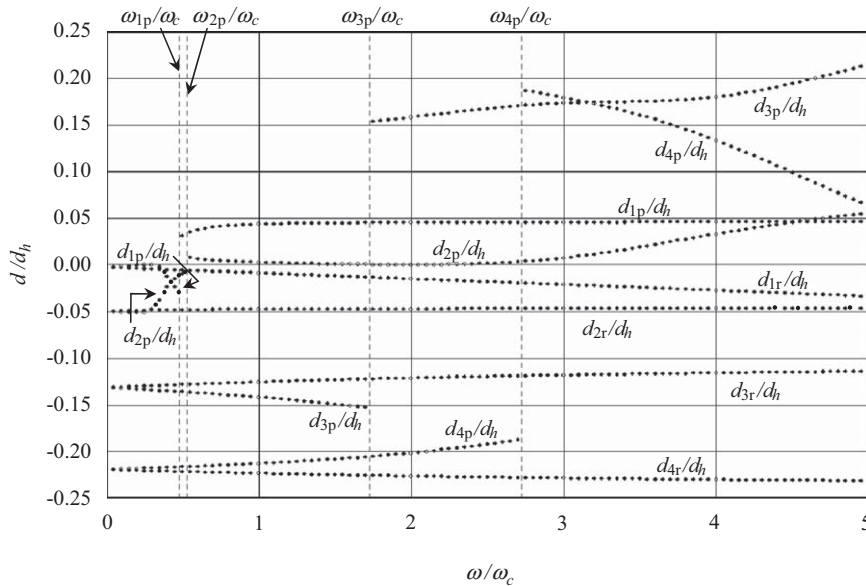


Fig. 8. Viscous damping needed to counteract the hysteresis destabilizing effect for various precession motions of a system without dry friction. Data: $K_3=K_4=1, M_3=M_4=0.5, J_d=0.15, J_a=0.1, d_1=d_2=d_3=d_4, L_3=0.3$. Subscripts 1, 2, 3, and 4 refer to the critical speeds, subscripts p and r refer to the progressive and retrograde precession speeds.

viscous-to-hysteretic damping ratio needed for stability. Clearly, when the minimum viscous damping needed to contrast the hysteretic instability comes out to be negative for some precession motion, this motion is certainly stable under the action of the hysteresis force alone.

The stability threshold of Fig. 8, where the viscous dampers are active and no dry friction is present, seems to be lower than in the stuck region of Figs. 4–6, where we have a complementary situation. Nevertheless, considering the larger number of damping sources present in the system of Fig. 8, the overall power dissipation may be regarded as being roughly the same.

The progressive critical speeds are also indicated in the diagram and it is remarkable that, for any one of them, an abrupt change of stability threshold occurs for the corresponding mode, due to the change of sign of $\Omega_n/\Omega - 1$.

Considering the symmetric case, $L_3=L_4=0.5$, $K_3=K_4=K_s$, $M_3=M_4=M_s$, $\delta_3=\delta_4=\delta_s$, and putting $\chi_1=1-\Omega_n^2$, $\chi_2=0.25-\Omega_n^2(J_d-J_a\Omega/\Omega_n)$, and $\chi_s=K_s+0.5-M_s\Omega_n^2$ for brevity, the characteristic equation for Ω_n can be found to be

$$\left[(1-\Omega_n^2) \left(K_s + \frac{1}{2} - M_s \Omega_n^2 \right) - \frac{1}{2} \right] \left[\left(\frac{1}{4} - J_d \Omega_n^2 + J_a \Omega \Omega_n \right) \left(K_s + \frac{1}{2} - M_s \Omega_n^2 \right) - \frac{1}{8} \right] = \left(\chi_1 \chi_s - \frac{1}{2} \right) \left(\chi_2 \chi_s - \frac{1}{8} \right) = 0 \quad (19)$$

Here, the first factor, $\chi_1 \chi_s - 1/2 = 0$, gives the cylindrical modes and the second one, $\chi_2 \chi_s - 1/8 = 0$, the conical modes. Then, calculating the cofactors of matrix \mathbf{Z}_0 , Eq. (18) becomes

$$\begin{aligned} & i\lambda \Omega_n \left[\chi_s \left(\chi_2 \chi_s - \frac{1}{8} \right) + \chi_s \left(\chi_1 \chi_s - \frac{1}{2} \right) \left(J_d - \frac{\Omega}{2\Omega_n} J_a \right) + 2M_s \left(\chi_1 \chi_2 \chi_s - \frac{\chi_2}{4} - \frac{\chi_1}{16} \right) \right] \\ & + \Omega_n \left[\chi_s \left(\chi_2 \chi_s - \frac{1}{8} \right) \delta_1 + \chi_s \left(\chi_1 \chi_s - \frac{1}{2} \right) \delta_2 + 2\delta_s \left(\chi_1 \chi_2 \chi_s - \frac{\chi_2}{4} - \frac{\chi_1}{16} \right) \right] \\ & + \operatorname{sgn} \left(\frac{\Omega_n}{\Omega} - 1 \right) \left[\chi_s \left(\chi_2 \chi_s - \frac{1}{8} \right) + \frac{1}{2} \left(\frac{\chi_2}{4} - \frac{\chi_1}{16} \right) + \frac{1}{2} \left(\chi_1 \chi_2 \chi_s - \frac{\chi_2}{4} - \frac{\chi_1}{16} \right) - \left(\chi_2 \chi_s - \frac{1}{8} \right) \right] = 0 \end{aligned} \quad (20)$$

where each value Ω_n implies the vanishing of either $(\chi_1 \chi_s - 1/2)$ or $(\chi_2 \chi_s - 1/8)$.

For the cylindrical modes, we must put $\chi_s = 1/(2\chi_1)$ into Eq. (20), which may be found to reduce to

$$i\lambda(1 + 2M_s \chi_1^2) + (\delta_1 + 2\delta_s \chi_1^2) + \Omega_n^3 \operatorname{sgn} \left(\frac{\Omega_n}{\Omega} - 1 \right) = 0 \quad (21)$$

It is thus observable that each retrograde precession ($\Omega_n < 0$) is certainly stable, even without viscous damping, while the progressive motions ($\Omega_n > 0$) are stable in the whole speed range $0 < \Omega < \infty$ if the condition $(\delta_1 + 2\delta_s \chi_1^2) > \Omega_n^3$ is satisfied. Notice the system instability in the supercritical range in the absence of viscous dissipation.

For the conical modes, we must put $\chi_s = 1/(8\chi_2)$ into Eq. (20), which changes to

$$i\lambda \left(J_d - \frac{\Omega}{2\Omega_n} J_a + 8M_s \chi_2^2 \right) + \delta_2 + 8\chi_2^2 \delta_s = 0 \quad (22)$$

Considering that $J_d - J_a \Omega / (2\Omega_n) = 0.5[J_d + (0.25 - \chi_2) / \Omega_n^2]$ by the definition of χ_2 and that $\chi_2 = 1/(8\chi_s)$ by the characteristic equation, Eq. (19), the factor of $i\lambda$ inside the brackets of Eq. (22) may be transformed, after some algebra, into $0.5J_d + [K_s + M_s \Omega_n^2 + 2(K_s - M_s \Omega_n^2)^2] / (16\chi_s^2 \Omega_n^2)$ and turns out to be always positive, whence all conical motions are stable.

6. Conclusion

The problem of hysteretic whirl instability in rotating machinery has to be solved by different approaches depending on linearity or nonlinearity of the system physical characteristics. For example, in the hypothesis of floating journal boxes with dry friction surfaces, planned to damp the critical speeds, the stability of periodic solutions with respect to small perturbations requires application of the Floquet theory, which implies the numerical calculation of the fundamental solution matrix, and the control that the characteristic multipliers are confined within the unitary circle of the Gauss–Argand plane. On the other hand, the nonlinear stability of rotor-shaft-bearing systems subject to dry friction in the supports requires numerical solution of the full equations. In the case of linear system with viscous damping, simpler straightforward procedures can be followed, leading to closed form results. The present analysis focused on these alternative methods and developed several applicative examples.

References

- [1] R.G. Kirk, E.J. Gunter, The effect of support flexibility and damping on the synchronous response of a single-mass flexible rotor, *ASME J. Engineering for Ind.* 94 (1972) 221–232.
- [2] R.G. Kirk, E.J. Gunter, Effect of support flexibility and damping on the dynamic response of a single-mass flexible rotor in elastic bearings, NASA CR-2083, July 1972.
- [3] Z. Guo, R.G. Kirk, Theoretical study on instability boundary of rotor-hydrodynamic bearing systems: part I—Jeffcott rotor with external damping, *ASME J. of Vibr. Acoust.* 125 (2003) 417–422.
- [4] Z. Guo, R.G. Kirk, Theoretical study on instability boundary of rotor-hydrodynamic bearing systems: part II—rotor with external flexible damped support, *ASME J. of Vibr. Acoust.* 125 (2003) 423–426.
- [5] F. Sorge, Rotor whirl damping by dry friction suspension systems, *Meccanica* 43 (6) (2008), 577–589.
- [6] F. Sorge, Damping of rotor conical whirl by asymmetric dry friction suspension, *Journal of Sound and Vibration* 321 (1–2) (2009) 79–103.
- [7] R.G. Kirk, H. Hornschuch, Bearing and housing assembly, US Patent no. 4119375, October 10, 1978.

- [8] D.C. Moringiello, S.H. Dallmann, Friction Damper, US Patent no. 4337982, July 6, 1982.
- [9] O. Montagnier, Ch. Hochard, Dynamic instability of supercritical driveshafts mounted on dissipative supports—effects of viscous and hysteretic internal damping, *Journal of Sound and Vibration* 305 (2007) 378–400.
- [10] H.L. Wettergren, On the behavior of material damping due to multi-frequency excitation, *Journal of Sound and Vibration* 206 (1997) 725–735.
- [11] O.N. Kirillov, Destabilization paradox due to breaking the Hamiltonian and reversible symmetry, *Journal of Non-Linear Mechanics* 42 (2007) 71–78.
- [12] F. Sorge, M. Cammalleri, An efficient damping technique for the unstable hysteretic rotor whirl by proper suspension systems, in: Proceedings of ECOTRIB 2009, European Conference on Tribology, Pisa, Italy, June 7–10, 2009.
- [13] J.P. Den Hartog, *Mechanical Vibrations*, McGraw-Hill B.C., New York, USA, 4th edition, 1956.
- [14] A.H. Nayfeh, D.T. Mook, *Nonlinear Oscillations*, John Wiley & Sons, New York, USA, 1979.